



ACADÉMIE
DES SCIENCES
INSTITUT DE FRANCE

Comptes Rendus

Géoscience

Sciences de la Planète

Nicolas Dall'Asta, Yoann Denèle, Vincent Regard, Anne Frayssignes, Guilhem Hoareau, Sylvie Leroy and Thibaut Pires

Analogue model of rift linkage and inversion with application to the Western Alps


Volume 356, Special Issue S2 (2024), p. 309-329

Online since: 20 September 2023

Part of Special Issue: Geodynamics of Continents and Oceans – A tribute to Jean Aubouin

Guest editors: Olivier Fabbri (Université de Franche-Comté, UMR CNRS 6249, Besançon), Michel Faure (Université d'Orléans-BRGM, UMR CNRS 7325, Institut des Sciences de la Terre, Orléans), Jacky Ferrière (Université de Lille, faculté des Sciences), Laurent Jolivet (Sorbonne Université, ISTeP, UMR 7193, Paris) and Sylvie Leroy (Sorbonne Université, CNRS-INSU, ISTeP, Paris)

<https://doi.org/10.5802/crgeos.231>

 This article is licensed under the
CREATIVE COMMONS ATTRIBUTION 4.0 INTERNATIONAL LICENSE.
<http://creativecommons.org/licenses/by/4.0/>



*The Comptes Rendus. Géoscience — Sciences de la Planète are a member of the
Mersenne Center for open scientific publishing*

www.centre-mersenne.org — e-ISSN : 1778-7025

Research article

Geodynamics of Continents and Oceans – A tribute to Jean Aubouin

Analogue model of rift linkage and inversion with application to the Western Alps

Nicolas Dall'Asta^{*,a}, Yoann Denèle^{*,b}, Vincent Regard^{*,b,c}, Anne Frayssignes^b,
Guilhem Hoareau^{*,a}, Sylvie Leroy^{*,d} and Thibaut Pires^b

^a Université de Pau et des Pays de l'Adour, E2S UPPA, CNRS, LFCR, France

^b GET, Université de Toulouse, CNRS, UPS, IRD, CNES, 14 av. E. Belin, F-31400
Toulouse, France

^c Department of Earth and Atmospheric Sciences & School of Natural Resources,
University of Nebraska-Lincoln, Lincoln, Nebraska, USA

^d Sorbonne Université, CNRS-INSU, ISTE, Institut des Sciences de la Terre de Paris,
France

E-mails: nicolas.dallasta@univ-pau.fr (N. Dall'Asta), yoann.denele@get.omp.eu
(Y. Denèle), vincent.regard@get.omp.eu (V. Regard), anne.frayssignes@univ-tlse3.fr
(A. Frayssignes), guilhem.hoareau@univ-pau.fr (G. Hoareau),
sylvie.leroy@sorbonne-universite.fr (S. Leroy), thibautpires31@gmail.com (T. Pires)

Abstract. Along-strike segmentation of orogens raises questions because its causes may predate orogeny in relation to structural inheritance. Here we focus on rift/margin linkage domains and their inversion by using analogue models with image analysis to extract the 3D strain field. Extensional models document, depending on the strike-perpendicular offset and the brittle-crust thickness, three types of rift linkage modes: (1) oblique linkage with early T-fault, (2) strongly-oblique linkage with R-fault network and, (3) transfer-linkage with late Y-strike-slip fault. Analogue model of inverted rift basins is used to analyse the misunderstood tectonic evolution of transition zones in the segmented Western Alpine belt.

Keywords. Rift linkage, Rift inversion, Inheritance, Analogue models, Strain field, Western Alps.

Manuscript received 11 January 2023, revised 30 July 2023, accepted 31 July 2023.

1. Introduction

As the continental lithosphere is very heterogeneous, rifts are rarely formed in straight lines but are more generally characterised by associations of rift segments separated by rift linkage zones. Numerical and analogue modelling highlighted a large variety of rift linkage structures that can be subdivided into two main groups, the accommodation zones (sometimes called relay ramps), in which deformation is

distributed and rift boundary faults do not connect, and transfer zones in which a localised fault zone connects rift segments [e.g., Acocella et al., 2005, Zwaan and Schreurs, 2017]. These two types of interactions are characterised as “soft linkage” and “hard linkage” [Walsh and Watterson, 1991], respectively. Several parameters have been identified as controlling rift linkage type and the development of specific structures. The large strike-perpendicular offset between rift segments promotes transfer zones to be narrower [Mauduit and Dauteuil, 1996, Dauteuil et al., 2002] or even prevent transfer zone de-

*Corresponding author

velopment leading to the formation of accommodation zones [Vendeville and Le Calvez, 1995, Autin *et al.*, 2010, Allken *et al.*, 2012, Le Pourhiet *et al.*, 2017, Neuharth *et al.*, 2021]. Accommodation zones development with overlapping geometry between rift segments is favoured by orthogonal rifting [Zwaan and Schreurs, 2017]. With increasing deformation [Acocella *et al.*, 2005] earlier accommodation zones can evolve into transfer zones through the creation of a large variety of rift linkage structures. The nature of the linkage structures is controlled in part by the overlap or underlap of rift segments at the beginning of oblique fault development [along-strike offset, Tentler and Acocella, 2010]. Noticeably, the rift linkage zone type depends also on the rift extension mode, whether wide, with numerous normal faults on each side, or narrow, with a restricted number of faults accommodating the deformation. The rift extension mode is dictated by the rheology of the crust/lithosphere [Buck, 1991, Buck *et al.*, 1999, Brun, 1999, Huisman and Beaumont, 2007]. Wide rift extension mode is favoured by a weak lithosphere that tends to prevent transfer zones to develop [Allken *et al.*, 2012, Zwaan *et al.*, 2016]. In a recent paper, based on high-resolution 3D numerical modelling, Neuharth *et al.* [2021] show that the key factors controlling the transition between hard and soft linkages are firstly the strike-perpendicular offset (x -offset) and secondly the strength of the continental crust [Neuharth *et al.*, 2021]. For a crustal configuration typical of the continental interior with a ratio of 25 km upper and 10 km lower crust, they define a typology of rift linkage in four regimes as the strike-perpendicular offset increases, from oblique linkage, transform linkage, microplate formation to rift jump. The first two types are examples of hard linkage, the last type of soft linkage. Microplate formation type, leading to the individualization of microcontinents, is an example of an accommodation zone evolving to a double transfer zone.

Mountain belts are particularly non-cylindrical, showing curved structures with along-strike variations in the timing and kinematics of major structures. These differences are related to variations in convergence velocities and finite shortening but also reflect the three-dimensional pre-structuration of the crust and lithosphere [i.e. structural inheritance, Mouthereau *et al.*, 2013, Bellahsen *et al.*,

2014]. Large-scale orogenic curvatures in the Tethyan (or Alpine-Himalayan) mountain belts, for example, such as the Alpine arc or the Himalayan oroclinal arcs are known to reflect indentation processes of the Adria microplate in Europe and Indian plate in Asia, respectively [Tapponnier *et al.*, 1986, Rosenbaum, 2014]. On a smaller scale, widespread evidences of along-strike segmentation seem to be partly controlled by the inversion of the segmented passive margins of the Neo-Tethys ocean and its oceanic branches such as the Alpine Tethys or the Valaisan in the Alpine orogen [e.g. Lemoine and Trümpy, 1987, Ribes *et al.*, 2019], as well as mature rifting domains as the lower-Cretaceous Pyrenean rift [Tugend *et al.*, 2015, Lescoutre and Manatschal, 2020]. In such orogenic belts, the inversion of offset syn-rift segments leads to specific structures, accentuating their non-cylindrical nature. Depending on the degree of reactivation of normal faults and of the counterpart propagation of thrust, specific structures, for instance footwall shortcut, break back thrust and thrust stacking of extensional imbricates, develop [e.g. Bonini *et al.*, 2012]. The 3D strain field of such systems needs to be investigated in a way to better restore and thus understand orogenic systems. Structural inheritance related to offset syn-rift segments inversion is indeed recognized to be a first-order parameter controlling Alpine-type orogenic growth [e.g., Mouthereau *et al.*, 2012, Bellahsen *et al.*, 2014], but is also one of the less known effects, often neglected for the sake of simplification.

In this paper we focus on the formation of offset rift basins but also more broadly of offset margin domains that form early during the rifting (proximal to inner necking zones). We are also concerned with inversion of these two types of systems during mature collision processes by accretion of poorly thinned continental crust subsequently to both early inversion of hyper-thinned rift or margin domains during immature collision (i.e. soft collision) and subduction processes which consumed the oceanic lithosphere. The purpose of this paper is to analyse the 3D strain field during extension and then inversion of offset rift segments with brittle analogue models. The Pelvoux–Mont-Blanc rift segments [Lemoine *et al.*, 1989, Ribes *et al.*, 2019, Dall'Asta *et al.*, 2022] in the Alpine orogen, will be compared to the models' extracted 3D strain fields during extension and inversion. By assuming that the 3D de-

formation field of rifts and poorly thinned margin domains and their inversion during mature collision phases is controlled by frictional processes involving the upper crust decoupled from underlying ductile processes, this cross analysis allows to integrate the first-order parameters that control the pre- to syn-orogenic evolution of the upper-brittle rheological level of orogens.

2. Model setup

We performed analogical experiments to determine the influence of kinematics on the geometry and localization of structures in rift linkage zones and the structural response when inverted during orogenic shortening. The design of the reference model in extension is inspired by the paleo-geodynamic reconstructions of the Western Alpine realm during lower-Jurassic early stages of rifting [Lemoine *et al.*, 1989, Pfiffner, 2014, Ribes *et al.*, 2019]. In these reconstructions, extension is defined to be orthogonal to rift segments and rift linkage zones at high-angle to the direction of rift segments, with x -offset less than 100 km (case of the Mont-Blanc/Belledonne transition zone) and greater than 100 km (case of the Pelvoux/Belledonne transition zone). Previous analogue modelling studies have shown that a high linkage angle (angle between segments and rift linkage) is favoured in the case of small along-strike offset [Tentler and Acocella, 2010], defined here as y -offset (Figure 1). That explains why we have chosen systems without underlapping or overlapping geometries between rift segments (e.g. y -offset = 0). The transient brittle–ductile transition is considered at a depth of 15 km with respect to previous studies of the Alpine Tethyan rifted margins [Mohn *et al.*, 2012]. The ratio length/thickness of the rift linkage domains is thus smaller or higher, respectively, than a value of 6.7.

To model the rift linkage zones during extension and inversion, we consider rift segments orthogonal to the divergence and then convergence directions and rift linkage zones are initially set up parallel to the displacements. The experiments consider the response of a 3 cm thick brittle layer to the deformation imposed at its base. The scaling factor with the Alps is thus 3 cm in the model representing 15 km in nature.

In the experiments, the length of the rift linkage zones is variable (10 and 20 cm, corresponding to length/thickness ratios of 3.3 and 6.7, respectively). These experiments are conducted on a large experimental table above which a metal plate is pre-cut into segments and rift linkage (Figure 1); the displacement was generated and controlled by a computer-driven stepper motor that pulled (or pushed during inversion) the plate at a constant rate.

We do not present all models here for simplicity, but rather illustrate the evolution of rift linkage domains from a representative model. To model the brittle crust, whose behaviour is of Mohr-Coulomb type [Byerlee, 1978], we use dry sand layers (quartz sand MI 0.1/0.35 from Sibelco; average grain size 0.26 mm (friction angle $\sim 32^\circ$, sand density $\sim 1.55 \text{ g/cm}^3$) for a total thickness of 3 cm. The inside layers have been coloured by adding colourant, which does not change the mechanical properties (Figure 1D). A passive grid of 5 cm wide tiles has been drawn on top of the sand pile (Figure 1B). The basal metal plate is shaped to create two rift linkage zones of length 10 and 20 cm, separating extension zones lying perpendicularly (Figure 1). The extension zones are 20 cm long (central basin), and >20 cm on both sides (outer basins), which prevents boundary effects. The model was extended by 4 cm before being inverted and shortened by 5 cm.

Model evolution was documented by top photos (Figure 1B), shot every 0.5 cm of deformation (0.25 cm in some cases). The characteristics of the top photos are unchanged throughout the experiment. The photographs were all rectified in the same way as the initial photo, which serves as a reference. For this one, the rectification was based on the grid drawn previously. We then documented the strain thanks to the tools PIVlab [Thielicke and Stamhuis, 2014] and Strainmap [Broerse *et al.*, 2021].

3. Results of analogue modelling

We describe in the following the reference experiment (label NDA03), but with additions from experiment NDA02, for cross-section interpretations (NDA02 is similar to NDA03, without inversion).

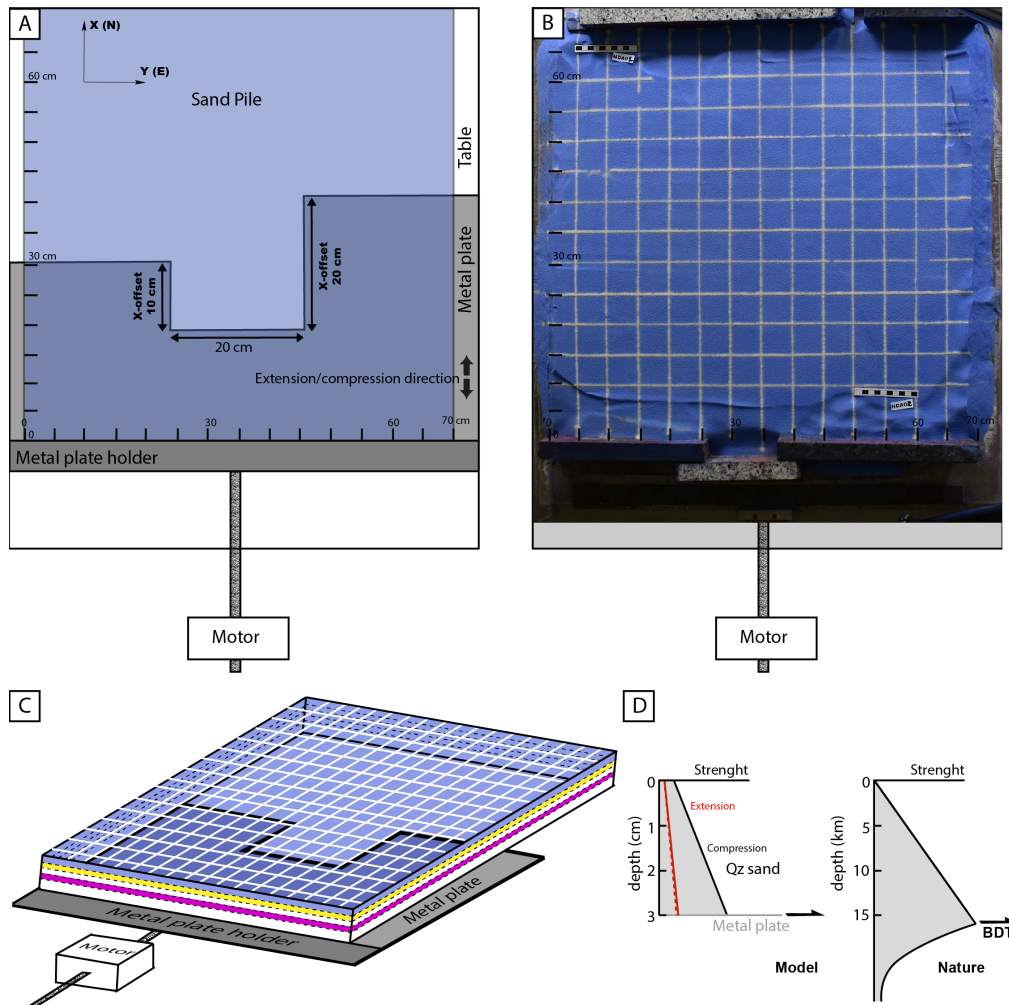


Figure 1. (A) Map view of the experimental set-up, only the dark grey area is moving. (B) Top photograph of the NDA02 experiment before the extension (note the passive grid of 5 cm wide tiles at the top of the model). (C) 3D view of the experimental set-up showing the colourful patterns of the sand pile. (D) Qualitative strength profiles in the model (left) and nature (right), BDT: Brittle–ductile transition.

3.1. Map view evolution of rift linkage zones during extension

The first strain increments lead to the opening of three basins bordered by two master normal faults in the rift segments. These conjugated normal faults are orthogonal to the extension direction. The structural evolution of the rift linkage zones occurred in three steps whose characteristics depend on the x -offset. In the initial step, deformation is diffuse. In the later steps, we observe two types of kinematic regimes: Type 1, connection through a strongly-oblique link-

age zone; Type 2, connection through a transfer linkage zone. These two types are described below, following observations reported in Figure 2.

3.1.1. Strongly-oblique linkage

After the initial step of diffuse deformation, the connection between the rift segments is visible on the surface of the model from 0.5 cm of extension. It takes place first in a localised manner on a Riedel-type oblique master fault (R-fracture [Riedel, 1929], with an angle of $\sim 30^\circ$ with the direction of

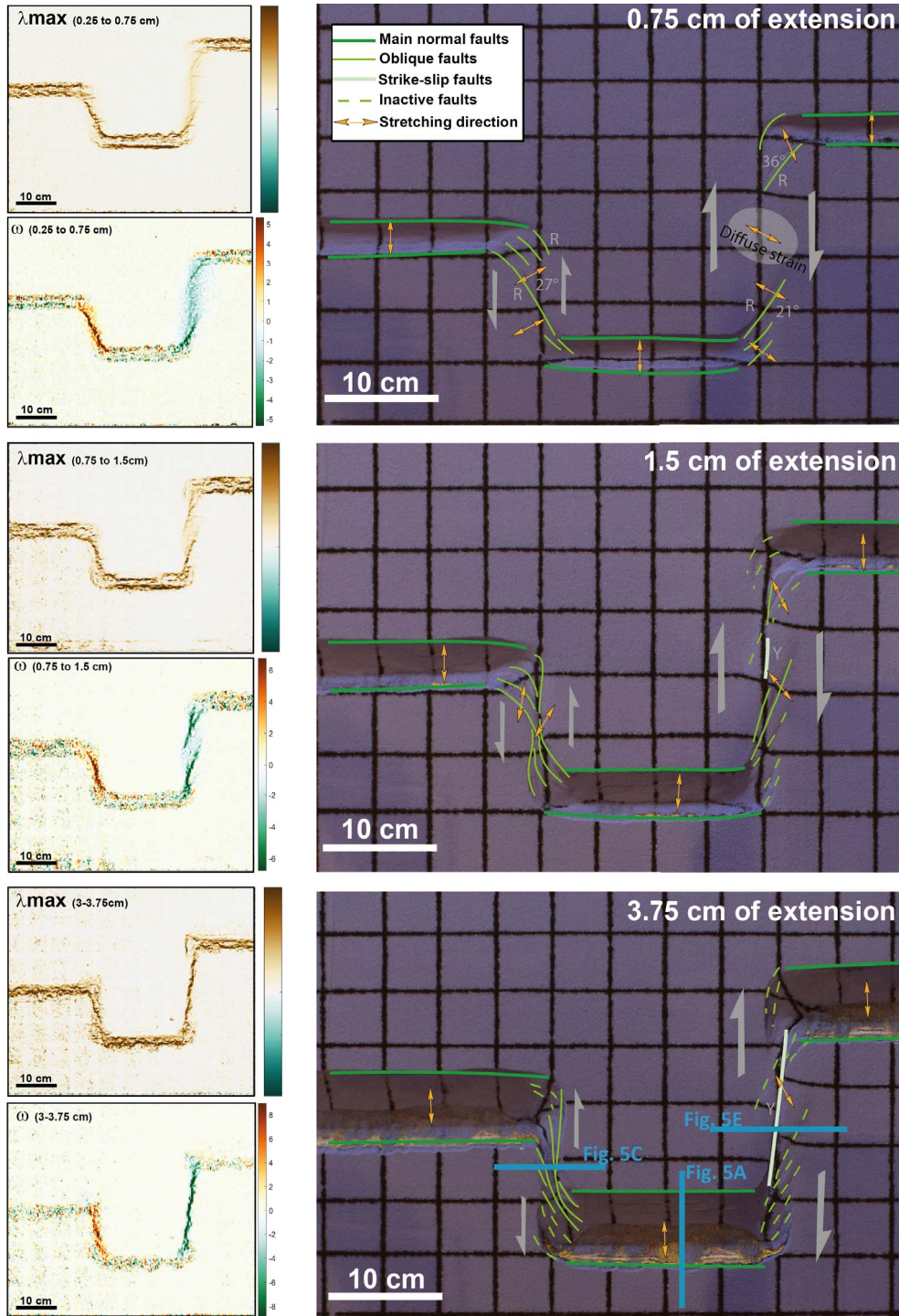


Figure 2. Interpreted pictures with stretching lineation directions extracted from strain map analysis (see Supplementary Material), principal strain axis stretch λ_{\max} ($\lambda = 1$ represents no length change), rotation ω (negative for clockwise and positive for anticlockwise) for the reference model NDA03. The dotted lines represent inactive faults.

extension, Figure 3), which creates a bridge between the inner parts of the rift segments. R-type control of the incremental bridge results in the formation of a linkage zone that is strongly oblique to the rift segments with a linkage angle of around 60°. We subsequently notice a progressive distribution of the deformation. This takes place first by development at the tip of the rift segments of multiple convex faults with both transtensional and strike-slip segments. The connection between the R-type master oblique fault and the multiple convex faults that spreads progressively inside, associated with clockwise/anticlockwise rotations that affect the outside part of rift segment tips, tends to enlarge the growing linkage zone and increase the linkage angle; those parameters reach 2 cm and 70° for 4 cm of extension. Strain is controlled by simple shear in the growing linkage, as shown by a highly oblique stretching direction (at an angle of 30°–60°) to the extension direction. Subsidence is initially strongly localised on the R-type fracture and the inside part of rift segment tips, then becomes more diffuse from 1.75 cm of extension with the propagation of depression areas from the curved tips of rift segments into the interior of the bridge, to cover the entire strongly-oblique rift linkage domain after 4 cm of extension.

3.1.2. *Transfer linkage*

The incipient bridge (0 to 0.5 cm of extension) between rifts segments is recorded by diffuse simple shear in the centre of the rift linkage zone (Figures 2 and 3). Multiple convex faults then develop (from 0.5 cm of extension) at the outside tips of the rift segment. From 1 cm of extension two master R-type oblique faults form from the inside tip of rifts segments and get connected from 1.25 cm of extension in the centre of the linkage domain by an incipient Y-type fault (i.e. parallel to the extension). From 1.5 cm of extension the deformation tends to localise on the master Y-fault that grows from the centre to the borders of the linkage domain; the Riedels and convex faults are left inactive. The final strike-slip structure is not exactly perpendicular to the rift segments: its strike differs by a few degrees (~12°). As in the strongly-oblique linkage domain, strain is controlled by simple shear and marked by a highly oblique stretching direction. The subsidence history is marked first by minor curved depression areas in

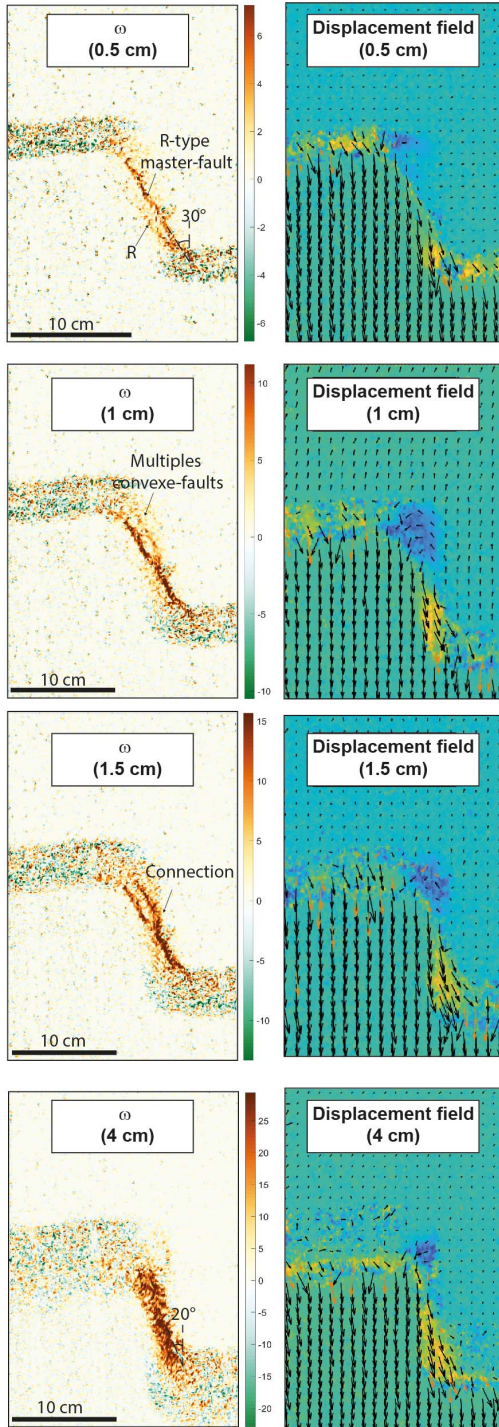
the inside tips of the segment and a large topographically high centre domain that develops until 1.5 cm of extension in a transpressive restraining bend localised between the two R-type faults. From 1.75 cm of extension, a localised depression alignment develops along the Y-fault trend which intersects the topographically high domain which persists on the edges of the fault up to 4 cm of extension.

3.2. *Map-view evolution during inversion*

Shortening only leads to the partial closure of the basins (Figure 4), as new thrusts develop outside the basins before basin closure (~3 cm of shortening). One consequence is that the depressions corresponding both to inherited rift segments and rift linkage zones are not removed and last up to the end of the experiment (5 cm of shortening).

The structural evolution during inversion occurs in two steps whose characteristics vary between initial rift segments and rift linkage zones. The first step is marked by passive folding related to distributed shortening in the core segments (Figure 4). The strongly-oblique linkage inversion occurs by a combination of neoformation of R-type dextral faults and inversion of the inherited convex faults (Figure 4). Interestingly, a rotation of up to 15° of the strike-slip fault is visible during shortening (clockwise for inherited strongly-oblique linkage, anticlockwise for inherited transfer linkage). At the same time, the strike-slip zone tends to become less localised. The transfer linkage zone is affected by sinistral strike-slip motion localised in the inherited dextral Y-type fault, associated with transpressive deformation in the inherited convex multiple faults at the tip of inherited rift segments (Figure 4). This deformation regime leads to the formation of a peculiar horse-tail fault geometry incompatible with the sinistral strike-slip motion that occurred during inversion. The second step of shortening takes place after ca. 3 cm of inversion and is associated with the neoformation of in-sequence thrust systems on both sides of the core segments and neoformed thrust-related lateral ramps centred on the inherited rift linkage domains (Figure 4). These lateral ramps gradually impose a widening of the inherited linkage zone by outward development, particularly visible at the end of the experiment for the strongly-oblique linkage.

Type 1 : Strongly oblique linkage



Type 2 : Transfer linkage

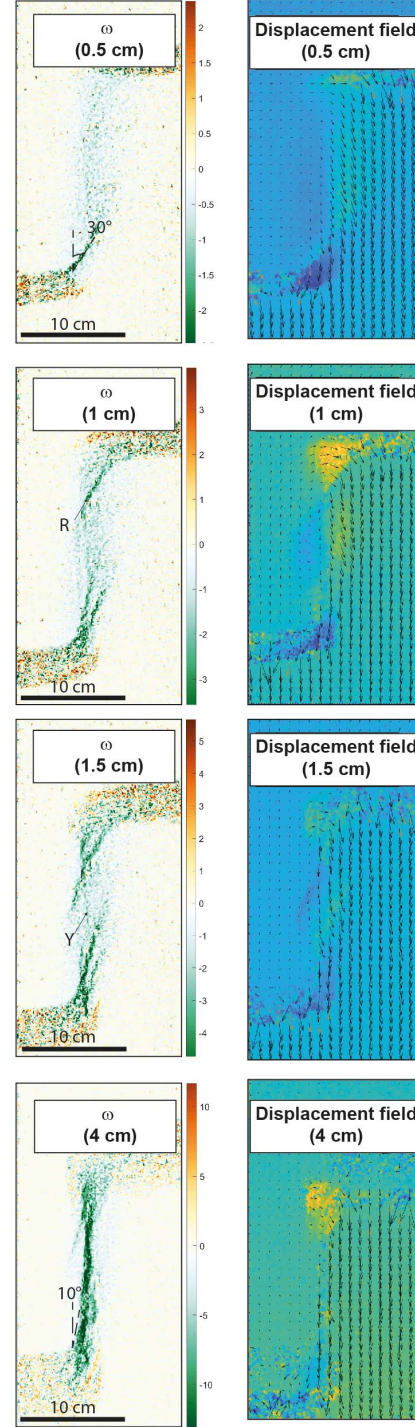


Figure 3. Rotation ω (negative for clockwise et positive for anticlockwise) and displacement field in the two rift linkage zones that develop in the NDA3 experiment.

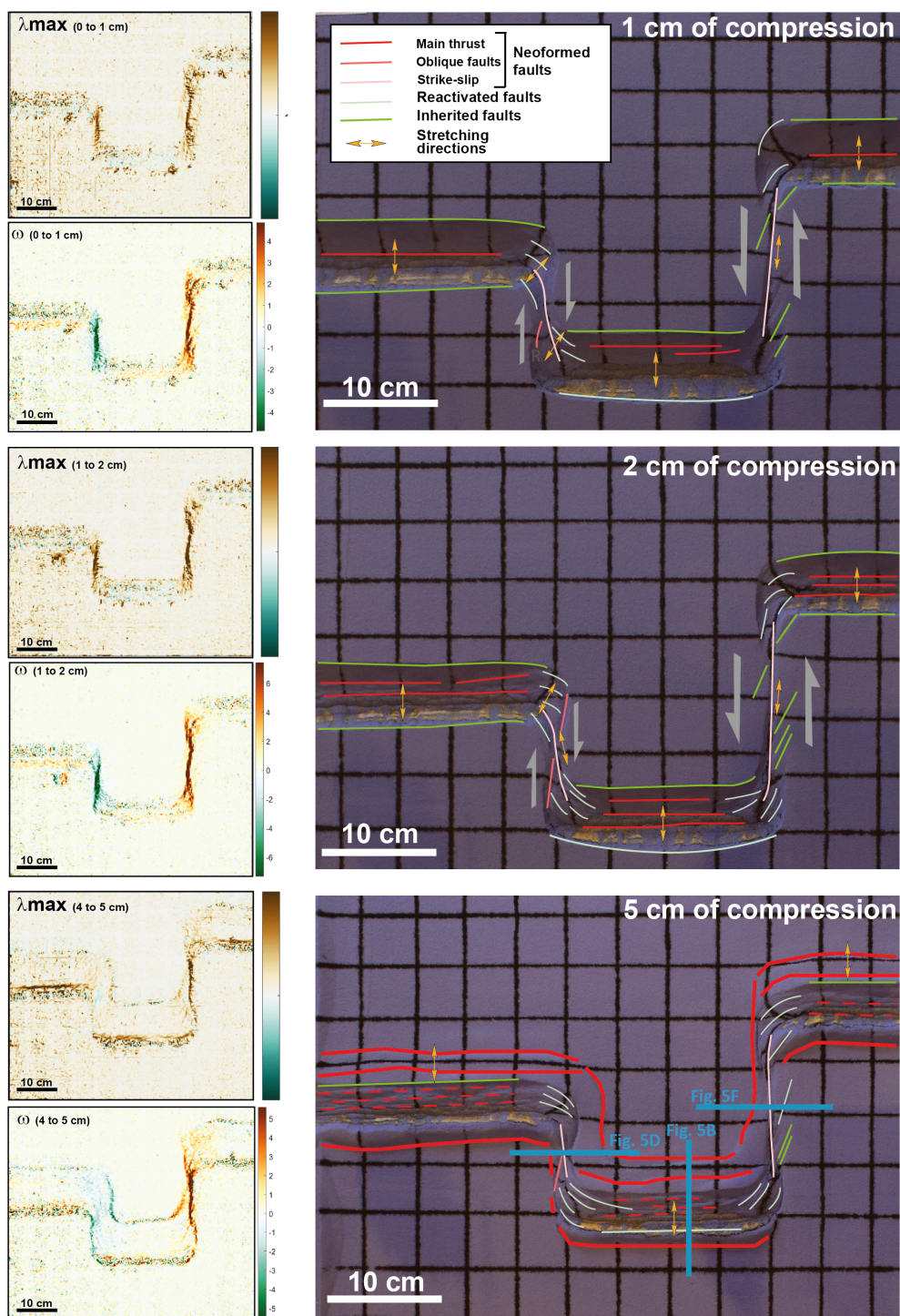


Figure 4. Interpreted pictures with stretching lineation directions extracted from strain map analysis (see Supplementary Material), principal strain axis stretch λ_{max} ($\lambda = 1$ represents no length change), rotation ω (negative for clockwise and positive for anticlockwise) for the reference model NDA03 during inversion.

3.3. Cross sections

3.3.1. Core segments

The extension is accommodated in core segments by a main normal fault (50°) that develops on the mobile metal plate and antithetic faults in its hanging-wall, in the fixed part of the sand pile; both accommodate only dip-slip motion. The antithetic faults develop in sequence as the basal metal plate moves; it leads to an asymmetric rift basin. While the main normal fault is active throughout the whole extension, each antithetic fault accommodates only part of the extension (Figure 5A).

During inversion, the master normal fault is first reactivated (1 in Figure 5B). The inner part of the core segment is squeezed in the middle against the major fault as shown by buttress folding. Then, when shortening increases, synthetic reverse faults form parallel to the main normal fault (2, 3, Figure 5B). This constitutes the short limb of an asymmetric inverted rift basin. The long limb is marked by shortcuts preserving part of the inherited normal faults (1' and 1'') and subsequent outward propagation of thrusts (2', 4, Figure 5B).

3.3.2. Rift linkage zones

Cross sections show steep faults branching at depth with small vertical displacements: they correspond to flower structures, whether positive or negative (case shown Figures 5C and E). The movement accommodated is mostly lateral, invisible in cross section and interpreted from map-view photographs.

The inversion in the inherited strongly-oblique linkage zone led to the formation of an imbricate structure composed of 3 thrust units (Figure 5D). These thrust units (1, 2 and 3) are smaller than in the core zone (Figure 5D). An apparently almost vertical fault accommodates most of the dextral strike-slip motion in the unit 1. Interestingly, parts of the steep faults inherited from the extension stage are preserved and transported passively on the nappes (units 1 and 2).

Within the inherited transfer linkage, it is interesting to note that faults developed during extension are clear: the outer faults are Riedel while steep faults near the centre are Y-planes (Figure 5E). The cross sections suggest that inversion mostly led to the reactivation of the Y-plane while Riedels show only minor

reactivation (Figure 5F). A lateral ramp is observed connecting the two main neoformed thrusts that develop in the fixed sand pile part of the core segment and accommodating most of the deformation in the transfer zones after 3 cm of inversion. These different sections show that preserved rift-related structures can be observed locally in the inherited rift linkage domains.

4. Discussion of the model

To better understand the strain field in fossil rift and margin systems now included in mountain belts we focus this part of the discussion on the results of the extensional models. The results of the model in inversion will be discussed by comparison with the Alpine case in the Western Alps. The main results of the models for the transfer zones (e.g., strain directions, subsidence evolution) are then applied to the Western Alpine case to try to highlight the influence of rift-related pre-Alpine transfer zones on the segmentation of the Alps.

In extension, for x -offset lower than 200 km (equivalent to 40 cm in our model) we reproduce the transition highlighted in numerical modelling, from oblique linkage to transfer linkage with a transfer zone almost orthogonal to rift segments [Neuharth *et al.*, 2021]. Our results also clearly show a decrease in the width of the linkage domain with increasing x -offset [Mauduit and Dauteuil, 1996]. Although the transfer linkage zone is similar to that obtained by Neuharth *et al.* [2021], the oblique linkage zone is significantly different in our reference model, with a larger initial linkage angle (60° vs. 25°) and a subsequent contrasting structural evolution. The linkage angle was recognized as being dependent on the first-order on the y -offset by Tentler and Acocella [2010] but this conclusion is challenged by the results obtained by Neuharth *et al.* [2021] which show very similar rift linkage domains for the y -offset between 100 and 400 km. Furthermore, it must be considered in natural examples that the y -offset is only a function of the propagation time of the rift segments, which is not the case for the x -offset. Le Pourhiet *et al.* [2017] and Neuharth *et al.* [2021] suggest a first-order control on the linkage angle by the crustal strength. The results of numerical models by Allken *et al.* [2012] with a brittle upper crust overlying a ductile lower crust show that hard

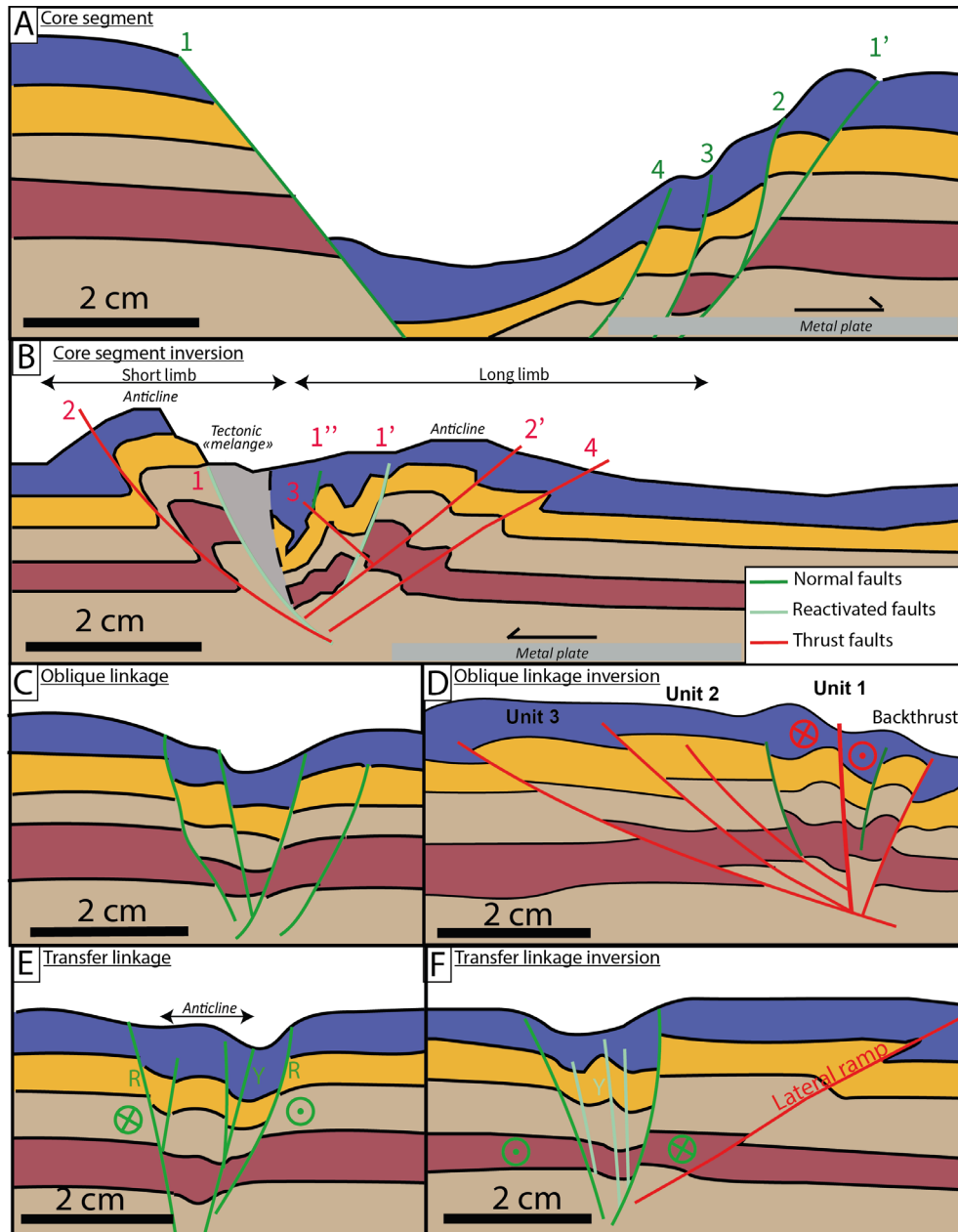


Figure 5. Line drawing of the cross sections after a 4 cm extension (panels A, C, E, experiment NDA02) and after a 5 cm inversion (panels B, D, F, experiment NDA03) with the addition of the photograph of the model for panel (B). The cross sections were cut at similar locations and the difference between the two cross sections of the same pair is assumed to represent the evolution during inversion. Green: faults active during extension; red: faults active during shortening; light green: reactivated faults. Numbers represent the time sequence of fault activation. Pair A and B: cross sections in core segments; pair C and D: cross sections in the middle of the strongly-oblique linkage; pair E and F: cross sections in the middle of the transfer linkage. The original photographs of the cross sections are available in Supplementary Figure 5.

linkage is favoured against soft linkage in the case of strong decoupling. For the case of weak coupling with a brittle crust decoupled from underlying deformation (closely similar to our models), these results suggest a first-order control on the linkage angle of the ratio (called here x_h ratio) between the x -offset and the thickness h of the brittle crust.

To better understand the control on linkage angle in the case of low x -offset (<200 km) we have tested the impact of various x_h ratios in other experiments, named NDA1 and NDA4 which are presented in Supplementary Material and synthesised in Figure 6. Our results show a clear control of the x_h ratio on the linkage angle. For low x_h ratio (<2.5) we reproduced the characteristics of the rift linkage (linkage angle of ca. 35°) obtained by Neuharth *et al.* [2021] for low x -offset: the linkage mode is oblique, controlled by the early development of T Riedel-type planes leading to a rapid connection between normal faults of the rift segments. For intermediate x_h ratio (2.5 to 4.5), strongly-oblique linkage development is controlled by the early formation of R Riedel-type planes. Finally, for a higher x_h ratio (>4.5), transfer-linkage development is controlled by the later formation of a Y Riedel-type fault. These 3 linkage modes, which are characteristic of low x -offset (<200 km) in decoupled crust, can be explained by a competition between simple shear accommodating deformation in the rift linkage zone and local stress variations around the main normal fault. For instance, the coseismic slip on normal faults is associated with a decrease of stress on the footwall and hanging-wall [Nüchter and Ellis, 2011, Thompson and Parsons, 2016], and a stress increase on the fault extremities, which can possibly drive fault propagation [King and Deves, 2015]. It appears that for a low x_h ratio, the local stress effects dominate and drive the propagation of the rift segments, favouring the formation of T-planes linking the two rift segments (Figure 6). For a higher x_h ratio, the rift linkage is dominated by simple-shear tectonics marked by the development of R and Y planes. Riedel shear fracture planes form and connect the two rift segments. The interaction between the Riedels and the main normal fault leads on the extremities to the rotation of the Riedel and the formation of convex faults. If the x -offset is too important, the Riedel faults can no longer connect the segments and there-

fore, the linkage will be achieved through the Y plane (Figure 6).

Our results, in accordance with high-resolution numerical models [Allken *et al.*, 2012, Neuharth *et al.*, 2021], show a first-order control of the x -offset and the x_h ratio on the mode of linkage. The three types of linkage modes defined here show contrasting records in terms of tectonic evolution and subsidence history. These results based on analogue modelling provide clues to better understand the structural record and the stratigraphic architecture of the basins of the highly-segmented fossil margins. Oblique linkages are marked by a rather rapid subsidence history (i.e., after a small amount of extension) with a depocenter that extends both from the centre of the linkage zone on normal faults (T-faults) and the tips of the segments. This type of linkage is also characterised by highly oblique faults that limit sub-basin domains and a stretching directed at 20° to 30° to the extension direction. The strongly-oblique linkage and transfer zones are marked by a very oblique stretching to the extensional direction (60° to 90°) attesting to strain control by simple shearing. Strongly-oblique linkage is marked by a network of two sets of faults, some with purely strike-slip kinematics and slightly oblique to the direction of extension and others with convex shapes and transtensional kinematics. Strongly-oblique linkage is marked by a depocentre that propagates from the segment tips towards the core which becomes a topographic low after about 2 cm of extension. In the transfer zones, the subsidence history is radically different, the linkage zone undergoes strong uplift up to 4 cm of extension, and only a small area intersected by the Y fault is in subsidence and only after 4 cm of extension. The structural record shows the interaction of 3 types of faults, purely strike-slip faults oblique to the direction of extension or parallel to the direction of extension and faults with a transtensional component with convex shapes.

5. Comparison of analogue models with the Western Alps (Pelvoux–Mont-Blanc segment)

This section discusses how our models provide a better understanding of the Pelvoux–Belledonne–Mont-Blanc segment in the Western Alps. Two possible rift linkage domains are described: the

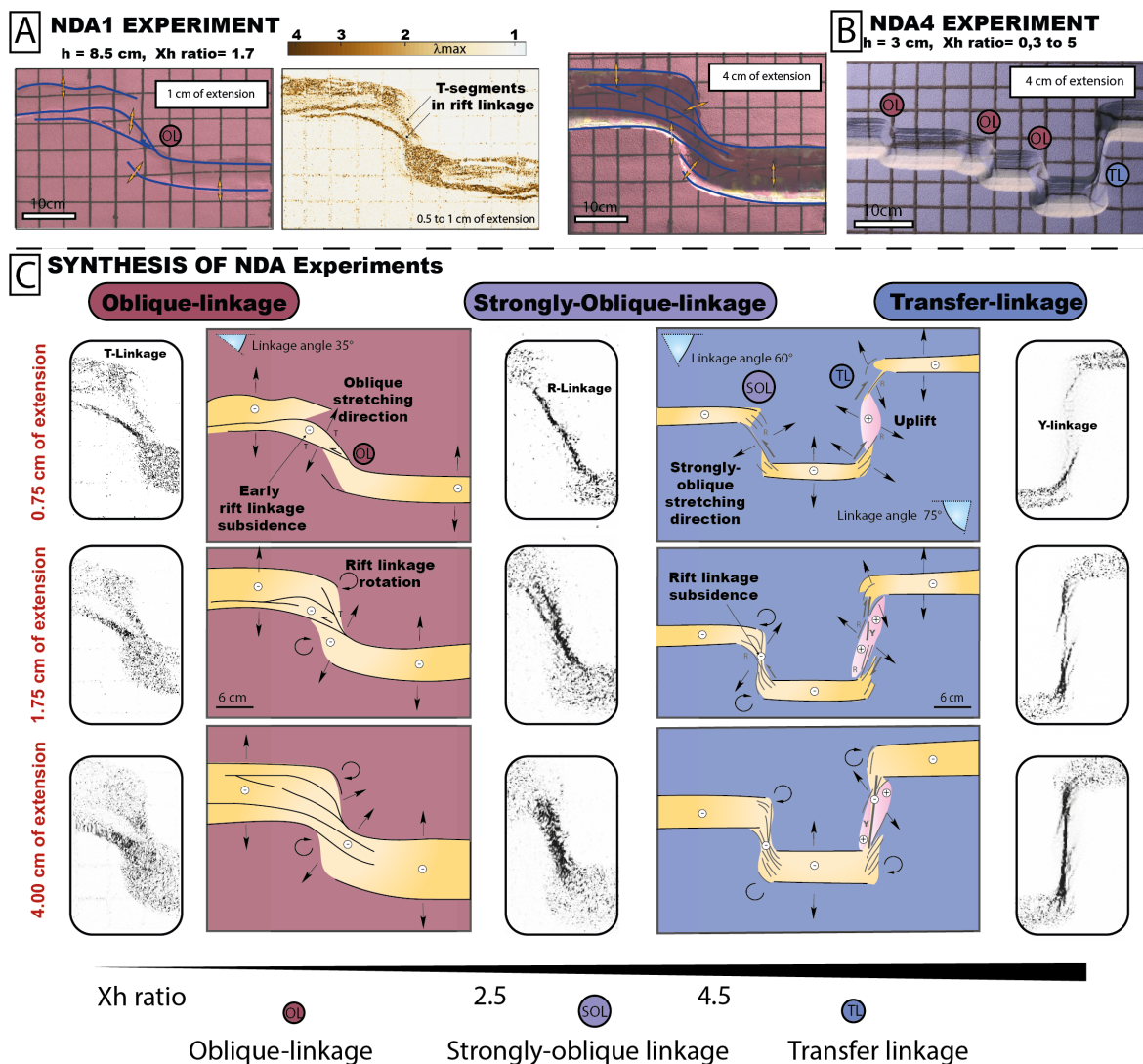


Figure 6. (A) Results of the NDA1 experiments ($h = 8.5$ cm, x -offset = 10 cm, x_h ratio = 1.2) after 1 cm and 4 cm of extension, principal strain axis stretch λ max is represented for the interval 0.5–1 cm of extension, (B) Results of the NDA4 experiment after 4 cm of extension ($h = 3$ cm, x -offset = 1, 2, 3, 5, and 15 cm, x_h ratio = 0.3, 0.7, 1, 1.7, and 5), (C) Synthesis of the NDA experiment with zooms representing the evolution of the ω parameter to illustrate first-order structures developing in rift linkage domains and structural schemes illustrating the evolution of the various rift linkage zones defined in this study (see text for explanations).

Pelvoux–Argentera transfer zone to the south and the Belledonne/Mont-Blanc transition zone to the north. The existence of these linkage domains is difficult to assess due to the strong Alpine deformation obliterating most of the rift-related structures. The now inverted rift linkage domain between

the Belledonne and Mont-Blanc External Crystalline Massifs is characterised by syn-rift stretching lineations highly-oblique to the direction of extension whose tectonic meaning remains unclear [Dall'Asta *et al.*, 2022]. We bring in the following new insights from analogue modelling.

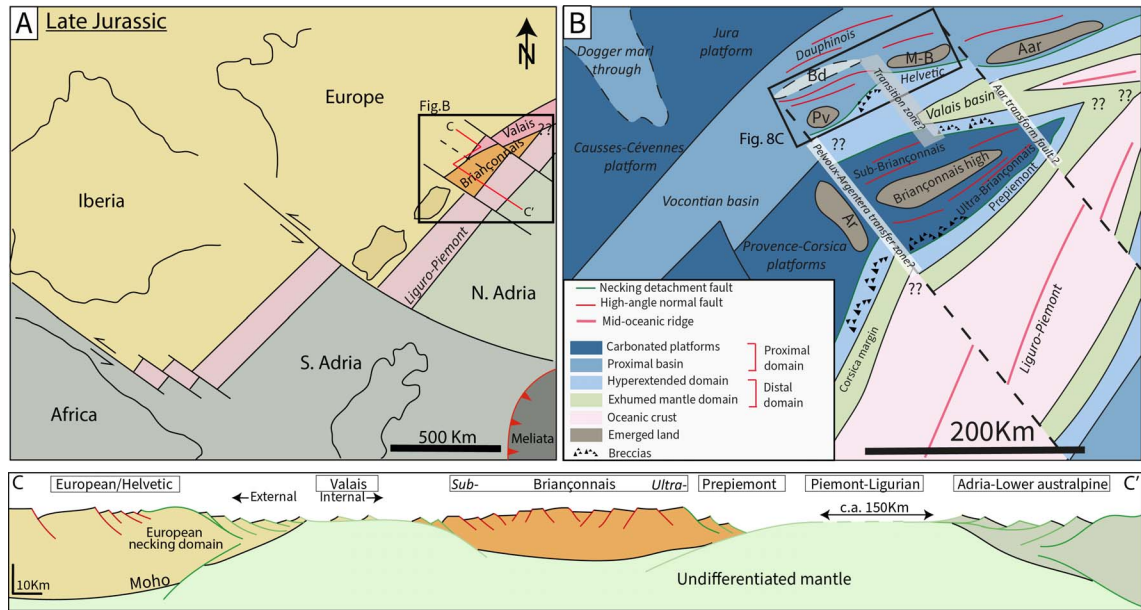


Figure 7. (A) Paleogeographic maps of Western Europe showing the location of the Liguro-Piemont and Valais oceanic basins during the Late Jurassic [based on Decarlis *et al.*, 2017]. (B) Proposal of a paleogeographic reconstruction of the Western Alps during the Late Jurassic showing the inferred transform systems in oceanic basins aligned with continental rift linkage domains [based on Lemoine and Trümpy, 1987, Lemoine *et al.*, 1989, Ribes *et al.*, 2019, Dall'Asta *et al.*, 2022]. Abbreviations for the External Crystalline Massifs: Ar: Argentera, Pv: Pelvoux, Bd: Belledonne, M-B: Mont-Blanc. (C) Cross-section of the Valais and Liguro-Piemont basins at the end of Jurassic [modified from Mohn *et al.*, 2012].

5.1. Geological setting

The Jurassic rifting in the Western Alpine realm is associated with the opening of two oceanic basins (Liguro-Piemont and Valais basin see Figure 7) separated by a continental ribbon (Briançonnais block). The area of interest corresponds to the Pelvoux–Belledonne–Mont-Blanc segment (ca. 170 km long, Figure 7B) of the inverted European margin bounded to the south by the inferred Pelvoux Argentera transfer/transform fault [Lemoine *et al.*, 1989] and to the north by the inferred Aar–Mont-Blanc transfer/transform fault. These faults correspond to syn-rift transfer zones and syn-spreading transform faults. Inside the Pelvoux/Mont-Blanc segment a lower-Jurassic rift linkage zone is proposed between the Mont-Blanc and Belledonne massifs [Pfiffner, 2014, Ribes *et al.*, 2019]. Rifting is recognized to be associated with NW–SE extension direction [Lemoine *et al.*, 1989, Le Breton *et al.*, 2021]. While the distal

part of the European and Adria margins have been widely studied, the transition between the proximal domain (25 ± 5 km-thick continental crust) and the hyperextended domain (<10 km continental crust) corresponding to the necking domain remain poorly constrained in the Western Alps (Figure 7C). It was proposed that the External Crystalline Massifs (ECM) and surrounding basins correspond to the former necking domain of the European margin [Mohn *et al.*, 2014].

The Jurassic margin was inverted during the Late Cretaceous [Ford *et al.*, 2006]. Inversion started with a subduction initiated in the Liguro-Piemont domain before a second subduction zone was created in the Valais during the Eocene [Rosenbaum and Lister, 2005]. Propagation of the deformation toward the continent led to the burial of the necking domain (e.g. ECM) under the accretion prism during the Late Eocene and Oligocene [Schmid and Kissling, 2000, Simon-Labric *et al.*, 2009, Cardello *et al.*, 2019],

followed by thick-skin deformation of the ECM during Oligocene and Miocene times [Herwegh and Pfiffner, 2005, Bellahsen *et al.*, 2012]. The shortening directions in the ECM are E–W to NW–SE [Gillcrist, 1988, Ford *et al.*, 2006], and orthogonal to the margin [Gillcrist, 1988]. Finally, late-stage NE–SW dextral strike-slip deformation in the ECM in relation to Late-Miocene Apulia rotation led to a clockwise rotation of the massifs [Gourlay, 1984, Hubbard and Mancktelow, 1992].

5.2. Comparison with models

5.2.1. Extension

In the External Crystalline Belledonne massif, Jurassic high-angle NE-striking normal faults have been recognized [Lemoine *et al.*, 1981, Barféty and Gidon, 1984, Chevalier *et al.*, 2003]. Although minor N–S extension is recorded in the massif, most extension is accommodated by two Late Liassic (Sinemurian) NE–SW faults, the Ornon and Mizoen faults [Gillcrist, 1988]. The Ornon fault is the best preserved and most studied of these faults (Figure 8C and D). It shows a NW–SE-directed syn-rift stretching direction [Gillcrist, 1988, Chevalier *et al.*, 2003], i.e. parallel to the direction of extension. Further north, Jurassic rift-related structures in the Aiguilles-Rouges/Mont-Blanc massif are more complex. The external Mont-Blanc corresponds to the termination of the Morcles basin where the sedimentary cover is pinched out [Epard, 1986] while the internal Mont-Blanc likely corresponds to a Jurassic detachment fault [Figure 8F, Ribes *et al.*, 2020, Dall'Asta *et al.*, 2022]. In the northern part of the detachment fault, stretching lineations are NW–SE-oriented (Figure 8B), parallel to the main extension direction and orthogonal to the normal faults as observed in the Western Alps.

Unlike these areas which are textbook cases (e.g., Ornon fault), unexplained strain fields can be observed. At the transition between the Mont-Blanc and Belledonne massifs for example, the southern part of the detachment fault shows a N–S stretching direction [Figure 8C; Col du Bonhomme; Dall'Asta *et al.*, 2022], oblique at an average of 45° to the NW–SE direction [Lemoine *et al.*, 1989]. In addition, the detachment fault is crosscut by NW–SE Jurassic high-angle normal faults showing a strike slip component. In this Mont-Blanc/Belledonne transition, the Beaufortain area is marked by specific rift-related

structures, which were proposed by Butler [1985] and Epard [1990] to be extensional imbricates forming small half-graben basins accommodating minor extension oblique to the main normal faults (Figure 8C and E). This fault architecture differs intriguingly from the central segments, both in terms of fault direction and offset. In this case, the analogue models we performed allow us to understand all the observations without the need to appeal to an exotic tectonic phase as an alternative hypothesis. Indeed, our analogue models strongly suggest that the oblique orientation of the stretching directions is one of the main characteristics of the oblique and transfer linkage modes. Interestingly, in the model, strongly-oblique linkage is characterised by the formation of R-type and convex faults connecting the two main segments. These observations indicate that the area localised between the northern Belledonne and southern Mont-Blanc might correspond to a strongly oblique linkage zone with a connection that bridges the Ornon fault and the Mont-Blanc detachment fault (Figure 8C). Noteworthy, a delay in the subsidence is observed between the Ornon fault and the Belledonne/Mont-Blanc transition based on the detailed stratigraphic description from the Ornon cover and Beaufortain area. On the Ornon fault (Belledonne segment), significant subsidence is observed during Hettangian and Sinemurian times [ca. 110 m/Ma, Chevalier *et al.*, 2003]. On the contrary, in the transition between the Belledonne and the Mont-Blanc, the subsidence was much lower until the Pliensbachian (ca. 13 m/Ma between Hettangian and Sinemurian). We observed that R-linkage is similarly associated with a delay in subsidence (Figures 6 and 8A and B) compared to the main segments. This further suggests the importance of the oblique linkage understanding from analogue models to explain the Belledonne–Mont-Blanc transition.

The southern termination of the Belledonne/Mont-Blanc segment corresponds to the Pelvoux–Argentera transform fault (Figure 8C). Although the kinematics of this domain is not well constrained, it was proposed by Gillcrist [1988], based on the inversion of Jurassic structure, that the termination of the transform was connected to the Ornon fault by a convex fault network forming the tip splay of the transform fault. The analogue models support this hypothesis: they display similar convex faults, on the tip of the transform segments making the connection

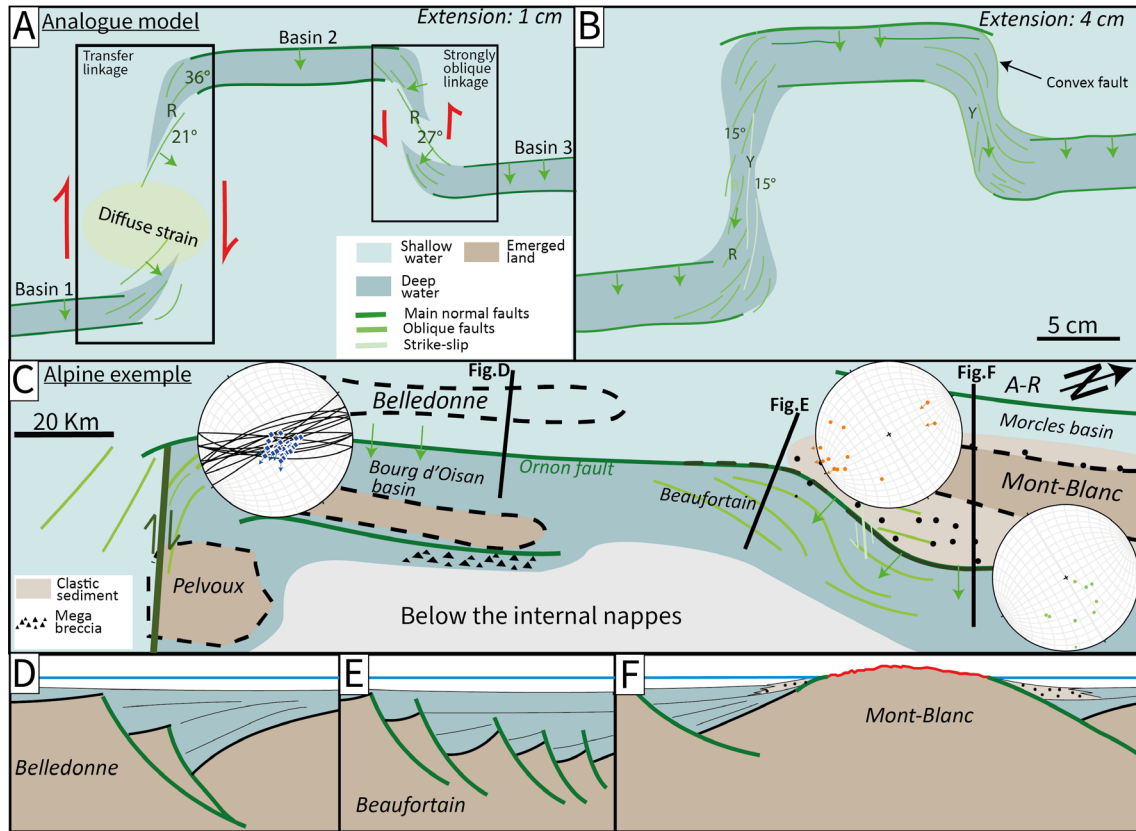


Figure 8. (A) Result of the analogue modelling for an extension of 1 cm. (B) Results of the analogue modelling for an extension of 4 cm. (C) Paleogeographic reconstruction of the Pelvoux–Mont-Blanc segment during the Late Jurassic [based on Lemoine *et al.*, 1989, Gourlay, 1984, Ribes *et al.*, 2019]. The stretching directions are from Gillcrist [1988] and Dall'Asta *et al.* [2022]. (D) Cross section of the Ornon fault [modified from Gillcrist, 1988]. (E) Cross section of the Beaufortain area [modified from Epard, 1990]. (F) Cross section of the Mont-Blanc massif.

with the main segments. Moreover, similarly to what is observed in models, the Pelvoux area underwent uplift during rifting [Roux *et al.*, 1988] which could be associated with the development of a transpressive restraining bend along the future transform fault.

In such Alpine Tethys examples, the initial localisation of the main rift segments (x and y -offset) might be related to the pre-rift structure of the crust (e.g., inherited crustal weakness). It is noteworthy that the Belledonne–Mont-Blanc (Beaufortain) linkage zone coincides with a change of basement lithology, from micaschist in the Belledonne massif to gneiss/granite in the Mont-Blanc massif, implying a different rheological behaviour of the basement crust.

5.2.2. Inversion

Some of the deformations observed in the inverted transfer zones of the model can be tentatively recognized in the Western Alps and could explain some of the early compressional features in the Beaufortain.

In detail, the reactivation/inversion of the core segments is well illustrated by the Bourg d'Oisans half-graben of Jurassic age (Figure 9B and D). The temperatures reached in the Belledonne massif during Alpine shortening favoured the development of large shear zones at ca. 30–25 Ma [Bellanger *et al.*, 2015]. These led to the closure of the half-graben and the extrusion of the syn-rift cover. In this case,

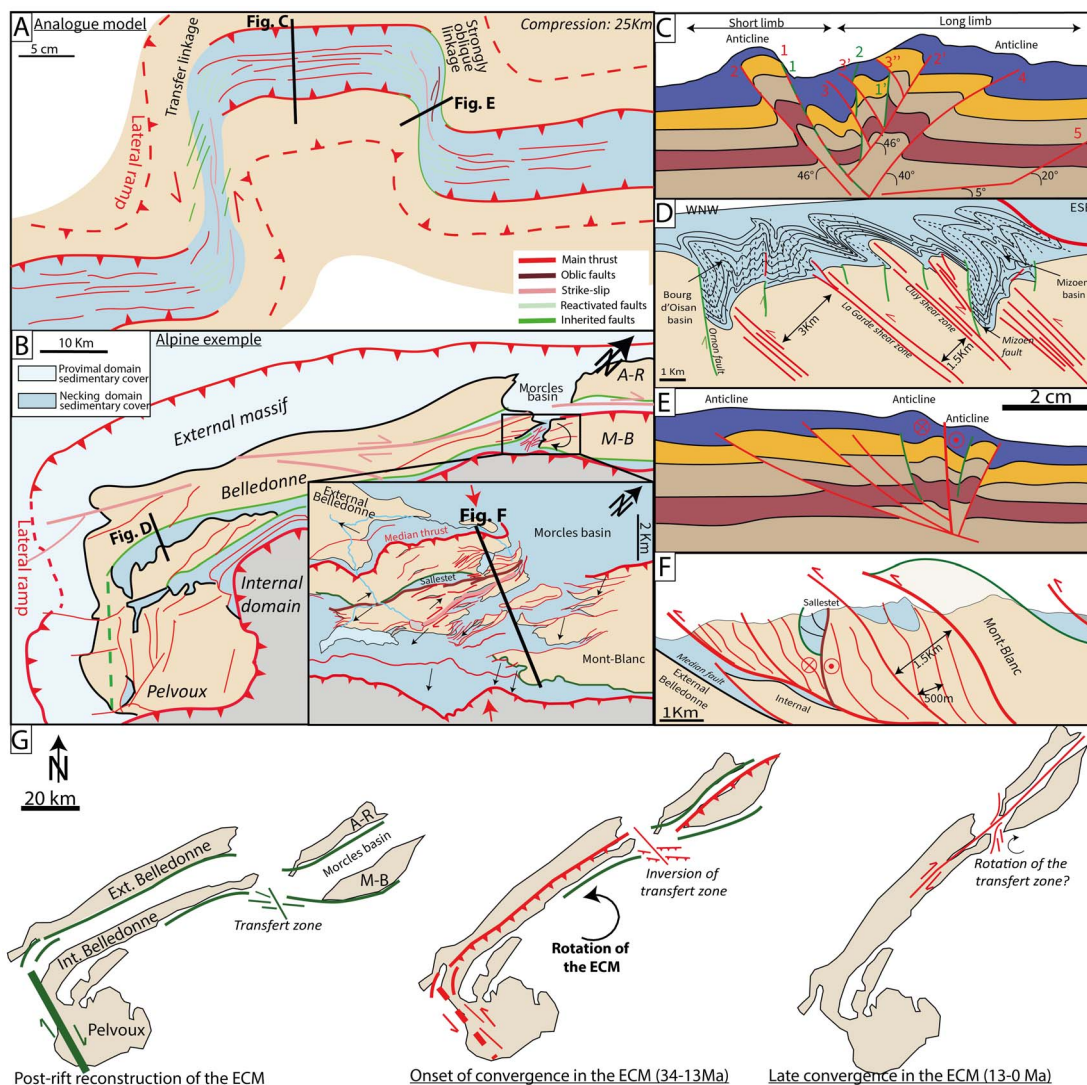


Figure 9. (A) Result of the analogue model showing the inversion of the core segment and linkage zones after 5 cm of shortening. (B) Simplified structural map of the Western Alps, focusing on the Beaufortain area between the Belledonne and Mont-Blanc massif. A-R = Aiguilles-Rouges, M-B = Mont-Blanc. The Maures massif located further south west of the Pelvoux is not represented. (C) Cross section of the core segment of the model. (D) Cross section of the Belledonne massif [from Bellahsen *et al.*, 2014]. (E) Cross section of the inverted growing linkage in the model. (F) Cross section of the Beaufortain area [modified from Eltchaninoff, 1980, and Butler, 1985]. (G) Evolution of the External Crystalline Massifs (ECM) from the end of the rifting to the convergence [based on Gourlay, 1984, Bellahsen *et al.*, 2014]. The collision is associated with the rotation of the ECM, the closure of the Morcles Basin and the inversion of the transfer zone in the Beaufortain and Pelvoux massifs.

the Jurassic Ornon fault acted as a buttress as highlighted by the strong vertical NE–SW foliation visible in the sediments close to the fault plane [Bel-

lahsen *et al.*, 2014, Figure 9D]. The deformation in the cover was mostly accommodated by flattening against the Jurassic fault. Similar deformation can be

observed in the Morcles basin between the Aiguilles-Rouges and Mont-Blanc massifs (Figure 8C), where it resulted in the extrusion of the syn-rift cover and the formation of the NE-striking Morcles nappe [Ramsay, 1981]. The comparison with analogue models suggests that pre-existing normal faults were only marginally inverted, and rather had a role of buttress (Figure 9C and D). This indicates a strong fault misorientation with respect to the inversion stress field. It also led to failure of the footwall forming short-cuts, and to the formation of break-back thrust in the hanging-wall [Boyer and Elliott, 1982, Figure 9]. It should be noted that the models seem to reflect well the natural case, in spite of the plastic deformation which prevailed in nature after the ECM (External Crystalline Massifs) were heated to a temperature higher than 300 °C following their burial under the internal nappes [Bellanger *et al.*, 2015].

The inversion of the linkage between the main segments is more complex. As proposed in the previous section, the Beaufortain might correspond to a strongly-oblique linkage domain connecting the Ornon fault and the Mont-Blanc detachment fault. Early deformation in the Beaufortain is marked by the presence of numerous thrusts oblique to the NE–SW thrust in the Mont-Blanc and Belledonne massifs, and showing N–S stretching directions associated with dextral strike-slip movement along the faults (Figure 9B). It corresponds to an early deformation associated with S1 foliation [Epard, 1990]. It was noticed by Epard [1990] that these faults do not cross-cut late Alpine folds, indicating that they are inherited and/or were active during early Alpine deformation, as also confirmed by ages as old as 14 Ma for N–S dextral shear in the Beaufortain [Egli *et al.*, 2017]. These faults constitute a nappe imbrication fan, contrasting with the Alpine structures organised into a crustal antiformal stack (Figure 9F). Some of these small nappes also correspond to an inverted Jurassic half-graben [e.g., Sallestet syncline; Epard, 1990]. In the area, late NE–SW strike-slip deformation occurred between the Mont-Blanc and Aiguilles-Rouges [since ca. 9 Ma Bergemann *et al.*, 2019], driving significant clockwise rotation [Figure 9G; Gourlay, 1984, Collombet, 2001, Delacou *et al.*, 2008]. The models we carried out allow us to overcome this late history. They teach us that the nappe imbrication, oblique with respect to the main direction of extension then shortening, is a completely natural

process if we consider that this zone is a rift linkage zone. This oblique deformation would therefore be contemporary to, and thus compatible with extension followed by shortening on the main segments considered here (Belledonne and Mont-Blanc).

Finally, we give a last example to convince that the rift linkages can express very oblique strain fields with respect to the directions of the surrounding structures: the Pelvoux–Argentera massifs. Indeed, the inversion of the transform in the Pelvoux led to the inversion of the splay in the Pelvoux massif associated with the formation of sinistral strike-slip faults [Gillcrist, 1988]. In addition, NW–SE lateral ramps (Figure 9B) connect the NE–SW thrust system of the Belledonne massif to thrusts systems of the Maures massif to the southwest.

Paired analogue models/structural analyses observations show that rift inheritance, especially in the rift linkage zones, can lead to complex kinematics during inversion. Some elements observed in the model such as the highly-oblique stretching in the linkage zone as well as the oblique faulting and subsidence can be observed in the Western Alps. This is particularly the case for the Beaufortain, highlighting the possible presence of a Jurassic transfer zone between the Mont-Blanc and Belledonne massifs. These observations might explain early Alpine deformations in the Beaufortain area, which still remain poorly understood. These simple analogue models might give new insight to better understand offset rift margins in the Alpine Tethys and their consequence on the subsequent collision.

6. Conclusion

In this study we show based on extensional analogue modelling that rift linkage between rift segments in the case of small x -offset (<200 km) in a brittle upper-crust mechanically decoupled for underlying structural levels, can occur in three modes. The oblique-linkage mode is characterised by the rapid connection between rift segments on a transtensional fault zone, and early subsidence history. The strongly-oblique linkage mode is marked by a progressive bridge formation by connections of strike-slip and convex transtensional faults, and a later history of subsidence. The transfer-linkage mode is driven by the late formation of an orthogonal strike-slip fault and characterised by the

formation of a large uplifted transpressional domain. We find that the x -offset and the ratio between the x -offset and the brittle crust thickness (called here x_h ratio) is the primary factor determining the connection mode. We also show that inversion of rift linkage domains leads to specific structural characteristics in inverted rift linkage domain combining the preservation of some inherited strike-slip faults, the formation of short-wavelength nappe stack decapitating early transtensional faults and neoformation of preferentially strike-slip faults.

When compared to the Alpine case, the analogue models succeed in illustrating how the main normal faults inherited from the rifting phase behave during inversion as buttresses squeezing post-rift sediments. But more significantly, the models address the problem of oblique deformation directions observed towards the terminations of the main rift segments. The models show us that the evidence of deformation oblique with respect to the main direction of extension then shortening, is a completely natural process if we consider that these zones are rift linkage zones. Such an oblique deformation is unquestionably compatible with the extension and inversion of the main segments, whose structures are inherited from the rifting phase. These results might give new insight to better understand offset rift margins and their consequence on subsequent collision not only in the Alpine Tethys but in other orogens worldwide.

Conflicts of interest

Authors have no conflict of interest to declare.

Acknowledgements

This work benefited from the financial support of E2S-UPPA to the first author. We benefit from the analogue modelling lab set up by F. Odonne [e.g. Dufr  chou *et al.*, 2011], whom we warmly thank. Benjamin Guillaume and Gianreto Manatschal are thanked for initiating us to PIVLAB and Strainmap analyses and discussions about the Alpine case, respectively. We would like to thank also the reviewer Franck Chanier and the editor Laurent Jolivet for the comments which helped to improve this manuscript.

Supplementary data

Supporting information for this article is available on the journal's website under <https://doi.org/10.5802/crgeos.231> or from the author.

References

- Acocella, V., Morvillo, P., and Funicello, R. (2005). What controls relay ramps and transfer faults within rift zones? Insights from analogue models. *J. Struct. Geol.*, 27, 397–408.
- Allken, V., Huismans, R. S., and Thieulot, C. (2012). Factors controlling the mode of rift interaction in brittle-ductile coupled systems: A 3D numerical study. *Geochem. Geophys. Geosyst.*, 13, article no. Q05010.
- Autin, J., Bellahsen, N., Husson, L., Beslier, M.-O., Leroy, S., and d'Acremont, E. (2010). Analog models of oblique rifting in a cold lithosphere. *Tectonics*, 29, 1–23.
- Barf  ty, J.-C. and Gidon, M. (1984). Un exemple de s  dimentation sur un abrupt de faille fossile. *Rev. Geol. Dyn. Geogr. Phys.*, 25, 267–276.
- Bellahsen, N., Jolivet, L., Lacombe, O., Bellanger, M., Boutoux, A., Garcia, S., Mouthereau, F., Le Pourhiet, L., and Gumiaux, C. (2012). Mechanisms of margin inversion in the external Western Alps: Implications for crustal rheology. *Tectonophysics*, 560/561, 62–83.
- Bellahsen, N., Mouthereau, F., Boutoux, A., Bellanger, M., Lacombe, O., Jolivet, L., and Rolland, Y. (2014). Collision kinematics in the western external Alps. *Tectonics*, 33, 1055–1088.
- Bellanger, M., Augier, R., Bellahsen, N., Jolivet, L., Moni  , P., Baudin, T., and Beyssac, O. (2015). Shortening of the European Dauphinois margin (Oisans Massif, Western Alps): new insights from RSCM maximum temperature estimates and $^{40}\text{Ar}/^{39}\text{Ar}$ in situ dating. *J. Geodyn.*, 83, 37–64.
- Bergemann, C. A., Gnos, E., and Whitehouse, M. J. (2019). Insights into the tectonic history of the Western Alps through dating of fissure monazite in the Mont Blanc and Aiguilles Rouges Massifs. *Tectonophysics*, 750, 203–212.
- Bonini, M., Sani, F., and Antonielli, B. (2012). Basin inversion and contractional reactivation of inherited normal faults: a review based on previous and new experimental models. *Tectonophysics*, 522–523, 55–88.

- Boyer, A. E. and Elliott, D. (1982). Thrust systems. *AAPG Bull.*, 66, 1196–1230.
- Broerse, T., Krstekanić, N., Kasbergen, C., and Willingshofer, E. (2021). Mapping and classifying large deformation from digital imagery: application to analogue models of lithosphere deformation. *Geophys. J. Int.*, 226, 984–1017.
- Brun, J.-P. (1999). Narrow rifts versus wide rifts: inferences for the mechanics of rifting from laboratory experiments. *Philos. Trans. Royal Soc. A*, 357, 695–712.
- Buck, W. R. (1991). Modes of continental lithospheric extension. *J. Geophys. Res. Solid Earth*, 96, 20161–20178.
- Buck, W. R., Lavier, L. L., and Poliakov, A. N. (1999). How to make a rift wide. *Philos. Trans. Royal Soc. A*, 357, 671–693.
- Butler, R. W. H. (1985). The restoration of thrust systems and displacement continuity around the Mont Blanc massif, NW external Alpine thrust belt. *J. Struct. Geol.*, 7, 569–582.
- Byerlee, J. (1978). Friction of rocks. *Pure Appl. Geophys.*, 116, 615–626.
- Cardello, G. L., Di Vincenzo, G., Giorgetti, G., Zwingmann, H., and Mancktelow, N. (2019). Initiation and development of the Pennine Basal Thrust (Swiss Alps): a structural and geochronological study of an exhumed megathrust. *J. Struct. Geol.*, 126, 338–356.
- Chevalier, F., Guiraud, M., Garcia, J.-P., Dommergues, J.-L., Quesne, D., Allemand, P., and Dumont, T. (2003). Calculating the long-term displacement rates of a normal fault from the high-resolution stratigraphic record (early Tethyan rifting, French Alps). *Terra Nova*, 15, 410–416.
- Collombet, M. (2001). *Cinématique et rotation des Alpes Occidentales. Approche paléomagnétique et modélisation analogique*. PhD thesis, Université Joseph Fourier, Grenoble. 137 pp.
- Dall'Asta, N., Hoareau, G., Manatschal, G., Centrella, S., Denèle, Y., Ribes, C., and Kalifi, A. (2022). Structural and petrological characteristics of a Jurassic detachment fault from the Mont-Blanc massif (Col du Bonhomme area, France). *J. Struct. Geol.*, 159, article no. 104593.
- Dauteuil, O., Bourgeois, O., and Mauduit, T. (2002). Lithosphere strength controls oceanic transform zone structure: insights from analogue models. *Geophys. J. Int.*, 150, 706–714.
- Decarlis, A., Beltrando, M., Manatschal, G., Ferrando, S., and Carosi, R. (2017). Architecture of the distal Piedmont-Ligurian rifted margin in NW Italy: Hints for a flip of the rift system polarity. *Tectonics*, 36, 2388–2406.
- Delacou, B., Sue, C., Nocquet, J.-M., Champagnac, J.-D., Allanic, C., and Burkhard, M. (2008). Quantification of strain rate in the Western Alps using geodesy: comparisons with seismotectonics. *Swiss J. Geosci.*, 101, 377–385.
- Dufréhou, G., Odonne, F., and Viola, G. (2011). Analogue models of second-order faults genetically linked to a circular strike-slip system. *J. Struct. Geol.*, 33, 1193–1205.
- Egli, D., Mancktelow, N., and Spikings, R. (2017). Constraints from $^{40}\text{Ar}/^{39}\text{Ar}$ geochronology on the timing of Alpine shear zones in the Mont-Blanc-Aiguilles Rouges region of the European Alps. *Tectonics*, 36, 730–748.
- Eltchaninoff, C. (1980). *Etude géologique entre Belledonne et Mont Blanc. La terminaison méridionale du massif du Mont Blanc et les terrains de son enveloppe*. PhD thesis, Université Pierre et Marie Curie-Paris VI. 196 p.
- Epard, J. L. (1986). Le contact entre le socle du Mont-Blanc et la zone de Chamonix: implications tectoniques. *Bull. Soc. vaud. Sci. Nat.*, 78, 225–245.
- Epard, J. L. (1990). *La nappe de Morcles au sud-ouest du Mont-Blanc*. PhD thesis, Université de Lausanne. 178 p.
- Ford, M., Duchêne, S., Gasquet, D., and Vanderhaeghe, O. (2006). Two-phase orogenic convergence in the external and internal SW Alps. *J. Geol. Soc. London*, 163, 815–826.
- Gillcrist, J. R. (1988). *Mesozoic basin development and structural inversion in the external Franch Alps*. PhD thesis, Imperial college, London. 430 p.
- Gourlay, P. (1984). *La Déformation alpine des massifs cristallins externes (Mont-blanc, Aiguilles rouges, Belledonne) et celle de leur couverture mésozoïque (Alpes occidentales)*. PhD thesis, Université Pierre et Marie Curie-Paris VI. 131 p.
- Herwegh, M. and Pfiffner, O. A. (2005). Tectono-metamorphic evolution of a nappe-stack: a case study of the Swiss Alps. *Tectonophysics*, 404, 55–76.
- Hubbard, M. and Mancktelow, N. S. (1992). Lateral displacement during Neogene convergence in the western and central Alps. *Geology*, 20, 943–946.

- Huisman, R. S. and Beaumont, C. (2007). Roles of lithospheric strain softening and heterogeneity in determining the geometry of rifts and continental margins. In Karner, G. D., Manatschal, G., and Pinheiro, L. M., editors, *Imaging, Mapping and Modelling Continental Lithosphere Extension and Breakup*, volume 282 of *Geological Society, London, Special Publications*, pages 111–138. Geological Society of London.
- King, G. C. P. and Deves, M. H. (2015). Fault interaction, earthquake stress changes, and the evolution of seismicity. In Schubert, G., editor, *Treatise on Geophysics*, volume 4, pages 225–255. Elsevier, Oxford, 2nd edition.
- Le Breton, E., Brune, S., Ustaszewski, K., Zahirovic, S., Seton, M., and Müller, R. D. (2021). Kinematics and extent of the Piemonte–Liguria Basin–implications for subduction processes in the Alps. *Solid Earth*, 12, 885–913.
- Le Pourhiet, L., May, D. A., Huille, L., Watremez, L., and Leroy, S. (2017). A genetic link between transform and hyper-extended margins. *Earth Planet. Sci. Lett.*, 465, 184–192.
- Lemoine, M., Dardeau, G., Delpech, P. Y., Dumont, T., de Grasciansky, P. C., Graham, R., Jolivet, L., Roberts, D., and Tricart, P. (1989). Extension syn-rift et failles transformantes jurassiques dans les Alpes Occidentales. *C. R. Acad. Sci. Paris*, 309, 1711–1716.
- Lemoine, M., Gidon, M., and Barfety, J.-C. (1981). Les massifs cristallins externes des Alpes occidentales : d'anciens blocs basculés nés au Lias lors du rifting téthysien. *C. R. séances Acad. Sci.*, 2, 917–920.
- Lemoine, M. and Trümpy, R. (1987). Pre-oceanic rifting in the Alps. *Tectonophysics*, 133, 305–320.
- Lescoutre, R. and Manatschal, G. (2020). Role of rift-inheritance and segmentation for orogenic evolution: example from the Pyrenean-Cantabrian system. *Bull. Soc. Géol. Fr.*, 191, article no. 18.
- Lacombe O. (Ed.) Special Issue Orogen lifecycle: learnings and perspectives from Pyrenees, Western Mediterranean and analogues.
- Mauduit, T. and Dauteuil, O. (1996). Small-scale models of oceanic transform zones. *J. Geophys. Res. Solid Earth*, 101, 20195–20209.
- Mohn, G., Manatschal, G., Beltrando, M., and Hapert, I. (2014). The role of rift-inherited hyper-extension in Alpine-type orogens. *Terra Nova*, 26, 347–353.
- Mohn, G., Manatschal, G., Beltrando, M., Masini, E., and Kuszniir, N. (2012). Necking of continental crust in magma-poor rifted margins: evidence from the fossil Alpine Tethys margins. *Tectonics*, 31, article no. TC1012.
- Mouthereau, F., Lacombe, O., and Vergés, J. (2012). Building the Zagros collisional orogen: timing, strain distribution and the dynamics of Arabia/Eurasia plate convergence. *Tectonophysics*, 532, 27–60.
- Mouthereau, F., Watts, A. B., and Burov, E. (2013). Structure of orogenic belts controlled by lithosphere age. *Nat. Geosci.*, 6, 785–789.
- Neuharth, D., Brune, S., Glerum, A., Heine, C., and Welford, J. K. (2021). Formation of continental microplates through rift linkage: numerical modeling and its application to the Flemish Cap and Sao Paulo Plateau. *Geochem. Geophys. Geosyst.*, 22, article no. e2020GC009615.
- Nüchter, J.-A. and Ellis, S. (2011). Mid-crustal controls on episodic stress-field rotation around major reverse, normal and strike-slip faults. In Fagereng, A., Toy, V. G., and Rowland, J. V., editors, *Geology of the Earthquake Source: A Volume in Honour of Rick Sibson*, volume 359 of *Geological Society, London, Special Publication*, pages 187–201. Geological Society of London.
- Pfiffner, O. A. (2014). *Geology of the Alps*. Wiley Blackwell, Oxford.
- Ramsay, J. G. (1981). Tectonics of the Helvetic Nappes. In McClay, K. R. and Price, N. J., editors, *Thrust and Nappe Tectonics*, volume 9 of *Geological Society, London, Special Publications*, pages 33–45. Geological Society of London.
- Ribes, C., Ghienne, J.-F., Manatschal, G., Dall'Asta, N., Stockli, D. F., Galster, F., Gillard, M., and Karner, G. (2020). The Grès Singuliers of the Mont Blanc region (France and Switzerland): stratigraphic response to rifting and crustal necking in the Alpine Tethys. *Int. J. Earth Sci.*, 109, 2325–2352.
- Ribes, C., Ghienne, J.-F., Manatschal, G., Decarlis, A., Karner, G. D., Figueredo, P. H., and Johnson, C. A. (2019). Long-lived mega fault-scarps and related breccias at distal rifted margins: insights from present-day and fossil analogues. *J. Geol. Soc.*, 176, 801–816.
- Riedel, W. (1929). Zur mechanik geologischer Bruchschainungen. *Zentralb. fur Mineral. Geol. Palaontol.*, 8, 354–368.

- Rosenbaum, G. (2014). Geodynamics of oroclinal bending: insights from the Mediterranean. *J. Geodyn.*, 82, 5–15.
- Rosenbaum, G. and Lister, G. S. (2005). The Western Alps from the Jurassic to Oligocene: spatio-temporal constraints and evolutionary reconstructions. *Earth Sci. Rev.*, 69, 281–306.
- Roux, M., Bourseau, J.-P., Bas, T., Dumont, T., de Graciansky, P.-C., Lemoine, M., and Rudkiewicz, J.-L. (1988). Bathymetric evolution of the Tethyan margin in the western Alps (data from stalked crinoids): a reappraisal of eustatism problems during the Jurassic. *Bull. Soc. Géol. Fr.*, 8, 633–641.
- Schmid, S. M. and Kissling, E. (2000). The arc of the western Alps in the light of geophysical data on deep crustal structure. *Tectonics*, 19, 62–85.
- Simon-Labric, T., Rolland, Y., Dumont, T., Heymes, T., Authemayou, C., Corsini, M., and Fornari, M. (2009). $^{40}\text{Ar}/^{39}\text{Ar}$ dating of Penninic Front tectonic displacement (W Alps) during the Lower Oligocene (31–34 Ma). *Terra Nova*, 21, 131–136.
- Tapponnier, P., Peltzer, G., and Armijo, R. (1986). On the mechanics of the collision between India and Asia. In Coward, M. P. and Ries, A. C., editors, *Collision Tectonics*, volume 19 of *Geological Society, London, Special Publications*, pages 115–157. Geological Society of London.
- Tentler, T. and Acocella, V. (2010). How does the initial configuration of oceanic ridge segments affect their interaction? Insights from analogue models. *J. Geophys. Res. Solid Earth*, 115, article no. B01401.
- Thielicke, W. and Stamhuis, E. (2014). PIVlab – towards user-friendly, affordable and accurate digital particle image velocimetry in MATLAB. *J. Open Res. Softw.*, 2, article no. e30.
- Thompson, G. A. and Parsons, T. (2016). Vertical deformation associated with normal fault systems evolved over coseismic, postseismic, and multi-seismic periods. *J. Geophys. Res. Solid Earth*, 121, 2153–2173.
- Tugend, J., Manatschal, G., Kuszniir, N. J., and Masini, E. (2015). Characterizing and identifying structural domains at rifted continental margins: application to the Bay of Biscay margins and its Western Pyrenean fossil remnants. In Gibson, G. M., Roure, F., and Manatschal, G., editors, *Sedimentary Basins and Crustal Processes at Continental Margins: From Modern Hyper-extended Margins to Deformed Ancient Analogues*, volume 413 of *Geological Society, London, Special Publications*, pages 171–203. Geological Society of London.
- Vendeville, B. C. and Le Calvez, J. (1995). Physical models of normal-fault relays between variably off-set grabens. *AAPG Bull.*, 79.
- Walsh, J. J. and Watterson, J. (1991). Geometric and kinematic coherence and scale effects in normal fault systems. In Roberts, A. M., Yielding, G., and Freeman, B., editors, *The Geometry of Normal Faults*, volume 56 of *Geological Society, London, Special Publications*, pages 193–203. Geological Society of London.
- Zwaan, F. and Schreurs, G. (2017). How oblique extension and structural inheritance influence rift segment interaction: insights from 4D analog models. *Interpretation*, 5, SD119–SD138.
- Zwaan, F., Schreurs, G., Naliboff, J., and Buiters, S. J. H. (2016). Insights into the effects of oblique extension on continental rift interaction from 3D analogue and numerical models. *Tectonophysics*, 693, 239–260.